Feature Article

Anti-Stokes cooling in semiconductor nanocrystal quantum dots:
A feasibility study (Yury P. Rakovich, John F. Donegan,
Mikhail I. Vasilevskiy, and Andrey L. Rogach, p. 2497)

Anti-Stokes cooling in semiconductor nanocrystal quantum dots: A feasibility study

Feature Article

Yury P. Rakovich[*,1]**, John F. Donegan**[1,2]**, Mikhail I. Vasilevskiy**[3]**, and Andrey L. Rogach**[4]

[1] School of Physics and CRANN Research Centre, Trinity College Dublin, College Green, Dublin 2, Ireland
[2] Principal Investigator, CRANN Research Centre, Trinity College Dublin, College Green, Dublin 2, Ireland
[3] Centro de Física, Universidade do Minho, Campus de Gualtar, Braga 4710-057, Portugal
[4] Photonics and Optoelectronics Group, Department of Physics and CeNS, Ludwig-Maximilians-Universitaet Muenchen, Amalienstr. 54, 80799 Munich, Germany

[*] Corresponding author: e-mail yury.rakovich@tcd.ie, Phone: +353 1 896 1821, Fax: +353 1 671 1759

In this review, we discuss the feasibility of laser cooling of semiconductor nanocrystal quantum dots by phonon-assisted anti-Stokes photoluminescence. Taking into account recent experimental advances, in particular, the development of semiconductor nanocrystals with very high quantum yield, we analyze in detail how the various physical processes in nanocrystals might help or hinder the cooling process. Possible experimental approaches to achieve efficient optical cooling are also discussed.

1 Introduction It has been long recognized that interaction of a fluorescent gas with radiation can lead to cooling of the gas when the electronic energy extracted by photon emission exceeds that introduced by photon absorption [1]. In contrast to the cooling of atomic ensembles by means of laser radiation pressure [2], laser cooling of condensed matter occurs in exceptional situations when the pump (absorption) frequency is lower than the mean luminescence frequency. This emission process is in violation of Stokes' law and is termed anti-Stokes photoluminescence (ASPL) and was first observed in dye solutions [3, 4]. It follows from energy conservation that the additional energy of the emitted photons in ASPL is taken out of the heat reservoir (i.e., illuminated material), which loses energy and, thus, cools. The absorption of vibrational energy distinguishes ASPL from other up-conversion effects like nonlinear two-photon excited luminescence. The thermodynamic viability of the anti-Stokes process was established by Landau [5] by considering the entropy of the incident and emitted light. It was shown theoretically that the entropy lost by the sample upon cooling can be compensated by an increase in the entropy of the light as a result of the loss of monochromaticity and beam directionality. Experimentally, however, such cooling by ASPL in the condensed phase is difficult to achieve and only lately conclusive results have been reported on successful cooling in rare-earth doped glasses and a fluid solution of a laser dye [6–8]. Even more recently, the cooling by more than 70 K has been attained using thulium-doped glass [9].

From a practical standpoint, however, it is far more desirable to achieve laser cooling in semiconductors, which are already being used in a variety of optoelectronic devices. The biggest potential advantage of semiconductors as compared to rare-earth doped materials is the ability to achieve optical cooling temperatures below 10 K [10]. This is due to the difference of the ground state populations in the two systems. As a consequence of the Boltzmann statistics, the population at the top of the ground state manifold of energy levels in a rare-earth doped system dramatically decreases as the temperature drops below 100 K, strongly reducing the efficiency of the cooling process. On the other hand, the population of energy levels in semiconductors is governed

Yury P. Rakovich received his diploma in Physics from the Belarusian State University and his PhD in physics from the National Academy of Sciences of Belarus in 1995. He worked as a lecturer in Physics at the Brest State Technical University until 1997 and moved to the University of Minho (Portugal) in 1998. He joined the School of Physics at Trinity College Dublin in 2001, where he works now as a senior research fellow at the Centre for Research on Adaptive Nanostructures and Nanodevices (CRANN). His current research focuses on optics of microcavities and photonic molecules, semiconductor nanocrystals and plasmonics.

John F. Donegan received BSc and PhD degrees from the National University of Ireland, Galway. He had postdoctoral periods at Lehigh University and the Max Planck Institute for Solid State Research, Stuttgart. He was appointed to the academic staff in Trinity College Dublin in 1993. He leads the Semiconductor Photonics Group and is Head of the School of Physics. He is also a principal investigator at the CRANN research institute in Trinity College Dublin. His research is in the area of Photonics, in particular the interaction of light with photonic structures: microspheres and photonic molecules coupled with nanocrystal emission, tunable laser structures based on slotted lasers, and two-photon absorption microcavity structures.

Mikhail I. Vasilevskiy was graduated from the Gorky State University in the USSR in 1981 and received his PhD in physics and mathematics from the same University in 1985. He worked as a lecturer and associate professor in physics at the N.I. Lobachevskii University of Niznii Novgorod (formerly Gorky) in Russia and had postdoctoral periods at the University of Essex (UK) and Universidade Federal Fluminense (Brazil). He moved to the University of Minho (UM, Portugal) in 1996, where he works now as a professor at the Physics Department and also is Head of Group of Physics Nanocrystalline Materials of the UM Centre of Physics. His current research is in the area of theory of the optical properties of semiconductor quantum dots and nanostructures.

by Fermi–Dirac statistics, which means that the lower energy valence band is populated even at temperatures close to absolute zero.

The fundamentals of laser cooling of semiconductors were considered in detail in the work of Sheik-Bahae–Epstein [10] where the range of parameters for which laser cooling is possible has been determined. Unfortunately, a number of issues make the laser cooling in semiconductors difficult to attain in practice. The main challenge is getting the cooling effects to dominate over heating. At low excitation intensities the heating is usually associated with non-radiative decay and multi-phonon emission. Therefore, high quantum efficiency is required to get net cooling. Another issue is low light extraction efficiency in bulk semiconductors and heterostructures, which is due to the high value of the refractive index. These challenges have so far prevented net cooling from being observed in semiconductor systems despite numerous experimental attempts [10–14].

It was recently suggested that the indicated problems can be significantly alleviated by employing quantum confinement nanostructures [10]. Due to the fact that the size of a nanostructure is smaller than the emission wavelength, the problem of light extraction is remedied. Moreover, in contrast to bulk semiconductors or heterostructures, the quantum efficiency of some nanostructures can be close to unity *at room temperature* [15, 16]. So far, a record efficiency of 99% has been observed in a GaAs/GaInP double heterostructure only by decreasing temperature down to 100 K [12]. These advantages along with the numerous recent reports on efficient ASPL [17–26] motivated us to gain insight into the feasibility of the proposed approach and requirements for achieving net laser cooling using one particular type of semiconductor nanostructures, namely nanocrystal quantum dots (QDs) fabricated via colloidal chemistry.

Andrey L. Rogach received his diploma in chemistry in 1991 and PhD in physical chemistry on synthesis and properties of silver nanoparticles in 1995 from the Belarusian State University in Minsk (Belarus). From 1995 to 1996 he was a postdoctoral fellow at the Institute of Physical Chemistry, University of Hamburg (Germany), where he also worked in 1997–2002 as a visiting scientist, Alexander-von-Humboldt Research Fellow, and finally staff scientist. Since 2002, he is a lead staff scientist at the Photonics and Optoelectronics group of the Ludwig-Maximilians-Universität in Munich (Germany). Since 2008, he is also an adjunct professor at the CRANN Research Centre of the Trinity College Dublin, Ireland, where he held an SFI Walton Award in 2005–2006.

These QDs represent the ultimate semiconductor-based quantum-confined system with atom-like energy levels, large optical transition dipole moment, and high photoluminescence (PL) quantum efficiency. The interest developed in nanocrystal QDs has been fueled by the high degree of reproducibility and control that is currently available in the fabrication and manipulation of these quantum-confined structures [16]. It is worth-mentioning that these QDs have been used in LEDs [27, 28], photonic [29, 30] and core–shell structures [31, 32], and as biological cellular probes [33, 34].

2 Basic principles of anti-Stokes refrigeration in solids The optical refrigeration can be achieved only in materials that have appropriately spaced energy levels and emit light with high quantum efficiency. To illustrate this concept we consider a system with a simple energetic structure including a ground state, which we denote "0", and an excited state, which consists of two closely spaced levels "1" and "2" (see Fig. 1).

For our aims we also assume that the spacing between the levels of the excited state, ΔE, could not be larger than a few kT, where k is the Boltzmann's constant and T is the temperature of the sample. This assumption guarantees the thermodynamical quasi-equilibrium between these two levels, which is established on a picosecond time scale after the carrier excitation. At the same time, the energy separation between the ground and exited states is supposed to be much bigger than ΔE. In this regime the effect of non-radiative transitions to the ground state can be neglected and carriers can only recombine from levels "1" and "2" by emitting a photon. In other words, the quantum yield (QY) of this model system is close to unity, i.e., nearly each absorbed photon results in a photon emitted by the system. Tuning the optical excitation to the transition energy "0"–"1" (Fig. 1), results in the overpopulation of the first excited level with respect to the population of the level "2" which is determined by thermal equilibrium. To restore the equilibrium, some electrons will be rapidly transferred to the highest level by absorbing phonons and, consequently, cooling the sample. This electron population will subsequently relax to the ground state by emitting photons with mean energy larger than that of the absorbed photons (Fig. 1). Evidently, luminescence from

both the level "2" and "1" will occur after the equilibrium is reached. The time scale of thermal interaction in bulk solids or nanostructures is in the picosecond regime, which is several orders of magnitude shorter than the time scale for optical transitions [35]. This means that the population distribution between the excited state levels reaches thermal equilibrium long before relaxing to the ground state. In the described process, the excess in the mean energy of the emitted photons over the absorbed ones is due to the thermal absorption required to equilibrate the excited levels and is carried out of the solid on the fluorescent light beam, resulting in cooling.

At thermal equilibrium, the population of the levels "1" and "2" follows the Boltzmann distribution. As the cooling process is driven by thermal energy extraction via the luminescence up-conversion, the carriers' recombination dynamics in the system presented in Fig. 1a can be described by the following set of coupled rate equations:

$$\frac{dn_1}{dt} = P - \left[\gamma_1 + \gamma_r \exp\left(\frac{-\Delta E}{kT}\right)\right] n_1 + \gamma_r n_2,$$

$$\frac{dn_2}{dt} = \gamma_r \exp\left(\frac{-\Delta E}{kT}\right) n_1 - \gamma_r n_2 - \gamma_2 n_2, \quad (1)$$

where n_1 and n_2 are the population densities of levels "1" and "2", respectively, $\gamma_1 (\gamma_2)$ is the recombination rate for transition "1" → "0" ("2" → "0"), and γ_r is the rate of relaxation "2" → "1".

Solving Eqs. (1) for continuous-wave excitation one obtains equations for both the resonant ($I_1 = \gamma_1 n_1$) and up-converted emission intensity ($I_2 = \gamma_2 n_2$)

$$I_1 = P \frac{c_1}{c_1 + A \, \exp(-\Delta E / kT)}$$

$$I_2 = P \frac{A \, \exp(-\Delta E / kT)}{c_1 + A \, \exp(-\Delta E / kT)}, \quad (2)$$

where the coefficients $c_1 = \gamma_1/\gamma_r$ and $A = \gamma_2/(\gamma_r + \gamma_2)$ are the ratios of the recombination rates. Note that these parameters can be estimated from the analysis of experimental PL decay curves [16, 36].

The first conclusion of this analysis is that the intensity of the up-converted emission is a linear function of the excitation power. Also resonant emission (transition "1" → "0") shows conventional thermal quenching (Fig. 2). However, the most pronounced feature of this model is that the intensity of the up-converted emission ("2" → "0") increases with temperature (Fig. 1b) by gaining energy from the thermal bath in contrast to the conventional quenching of resonant or Stokes-shifted photoluminescence (SSPL) with increasing temperature. As follows from Eq. (2), at high excitation intensity and/or at elevated temperatures (150–300 K), the temperature dependence of the ASPL intensity can be modeled by a single exponential growth function if $c_1 \gg A$. It is noteworthy that the energy gap
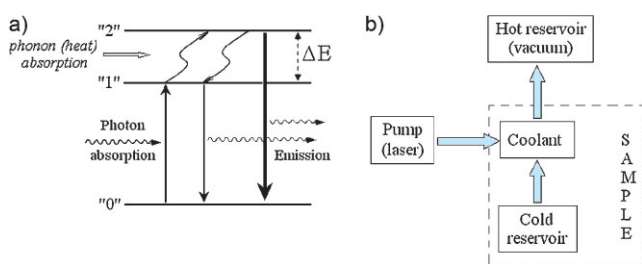
Figure 1 (online color at: www.pss-a.com) Schematics of (a) anti-Stokes optical cooling and (b) generalized refrigeration process.
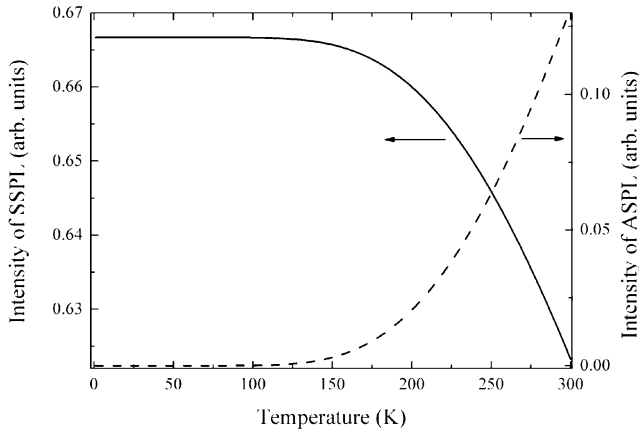
Figure 2 Temperature dependence of the intensities of Stokes shifted PL (solid curve) and ASPL (dashed curve) calculated according to Eq. (2) using $\Delta E = 100$ meV and values of recombination rates $\gamma_1 = \gamma_2 = 0.1 \times 10^9$ s^{-1} and $\gamma_r = 0.01 \times 10^9$ s^{-1}.

value ($\Delta E = 100$ meV) used in our model (Fig. 2) is larger than the highest phonon energy in any semiconductor material. This fact along with the exponential functional form of the probability for ASPL and SSPL excitations with respect to ΔE, means that the anti-Stokes cooling process is provided by the absorption of multiple phonons. This "anomalous" temperature behavior of the ASPL intensity may, therefore, be used as an indicator of phonon-assisted processes while analyzing the mechanisms of up-converted luminescence in materials. The growth of the ASPL intensity (and, therefore, the cooling efficiency) is clearly stronger at elevated temperatures (Fig. 2). Below 100 K, a high excitation intensity would be required in order to provide an appropriate level of cooling.

It is noteworthy that the energy level structure presented in Fig. 1a is just one of a number of possible schematics for cooling. Generally, a cooling system consists of both a ground state and an excited state, well separated from each other in energy, with at least one of the states split into two or more levels [37].

The thermodynamical processes in this kind of refrigerator have been considered in great detail by Mungan and Gosnell [37]. An optical cooling device can be analyzed in terms of a general refrigeration process similar to that shown in Fig. 1b. The energy and entropy flow from the pump source (e.g., a laser). Heat is extracted by coolant from the cold reservoir. In the case of laser cooling of solids, the coolant and cold reservoir are the same object, i.e., the sample with levels "1" and "2" coupled through phonon-mediated transitions (Fig. 1a). Energy and entropy are output to the hot reservoir (vacuum at $T = 0$ K), with the coolant experiencing changes in energy and entropy. The maximum energetic efficiency ($\eta_{\max}$) of this cooling process can be estimated considering a steady-state reversible operation of the coolant. As is typical for a reversible process, the equation for the efficiency can be simplified by substituting for the pump and hot reservoir temperatures in terms of level population, which

gives [38]

$$\eta_{\max} = \frac{\Delta E}{E_{\mathrm{abs}}}, \tag{3}$$

where E_{abs} is the energy of the pump transition from level "0" to "1". In other words, we can consider the process as a cooling cycle where the absorption of energy E_{0-1} causes the extraction of energy ΔE.

The cooling can also be quantified in terms of quantum efficiency (η_q) and the cooling power P_{cool}. In systems with a near-unity QY the cooling energy per photon is determined by the difference between the average energy of an emitted photon (E_{PL}) and the value of E_{abs}, with the corresponding wavelengths $\lambda_{\mathrm{PL}} = hc/E_{\mathrm{PL}}$ and $\lambda_{\mathrm{abs}} = hc/E_{\mathrm{abs}}$. According to an empirical rule known as Vavilov's law, the λ_{PL} and QY are independent [39] (or almost independent [40]) of the excitation wavelength in the optical spectral region of luminescence. For the excitation in the anti-Stokes PL regime, the emitted photons have higher energy than the absorbed ones. In this case the average cooling energy per photon in one cycle is given by

$$E_{\mathrm{cool}} = \eta_q E_{\mathrm{PL}} - E_{\mathrm{abs}} = \eta_q (E_{\mathrm{PL}} - E_{\mathrm{abs}}) - (1 - \eta_q) E_{\mathrm{abs}}. \tag{4}$$

From Eq. (4) we can obtain an expression for the cooling efficiency (η) defined as the ratio of the cooling power to the absorbed power

$$\eta = \frac{\lambda_{\mathrm{abs}} - \lambda_{\mathrm{PL}}^*}{\lambda_{\mathrm{PL}}^*}, \tag{5}$$

where $\lambda_{\mathrm{PL}}^* = \lambda_{\mathrm{PL}}/\eta_q$.

Equation (5) enables one to calculate the cooling efficiency for any given material using just experimental spectroscopic parameters. Also, Eqs. (4) and (5) help the understanding of why the anti-Stokes cooling is so difficult to obtain in practice. Indeed, the requirement for positive cooling efficiency ($\eta > 0$) implies $\eta_q > \lambda_{\mathrm{PL}}/\lambda_{\mathrm{abs}} \approx 1 - kT/E_{\mathrm{abs}}$. On the other hand, the value of E_{abs} must be sufficiently high ($\sim 20kT$) in order to minimize the multi-phonon relaxation [37]. This imposes strong restrictions on the QY value, which must be close to unity (desirably at room temperature where the ASPL efficiency is higher). Among all semiconductor materials, only colloidal QDs satisfy this condition [16, 41].

From Eq. (5), we can conclude that the larger the difference between the ASPL maximum and the excitation wavelengths, the higher will be the efficiency of the emitter used in the cooling system. For dye molecules or rare-earth elements there are limitations for increasing the excitation wavelength because it leads to a strong decrease of the absorption coefficient. We will discuss this point for the case of QDs in Section 3.4.

Phys. Status Solidi A **206**, No. 11 (2009)

2501

Feature

Article

3 Phonon-assisted anti-Stokes photoluminescence in nanocrystal quantum dots (state of the art)

3.1 General requirements for anti-Stokes cooling From the above discussion, we can formulate some general requirements for QDs with respect to anti-Stokes PL as the operating principle for laser refrigerators:

(1) Appropriate electronic structure with ground and excited states well separated from each other in energy, with the excited state split into two closely spaced levels.
(2) Strong electron–phonon and hole–phonon interactions to ensure high rate of absorption of lattice phonons.
(3) High PL QY in order to minimize the dissipation of the photon energy through sample heating due to non-radiative transitions.
(4) Independence of the emission properties of the excitation wavelength.
(5) Growth of the ASPL intensity with temperature.

In the next sections, we shall consider how these five requirements are met in nanocrystal QDs.

3.2 Electronic structure of QDs In the strong confinement regime (QD size < 10 nm), colloidal QDs exhibit an atomic-like structure of energy levels (Fig. 3a). The optical properties of excitons[1] confined in semiconductor nanocrystal QDs are often approximated by a two-level system [42] which, however, is not sufficient to explain a number of optical phenomena such as the Stokes shift of selectively excited luminescence, the long-lived QD emission, and the magnetic field dependence of the emission decays [43, 44]. A more realistic description takes into account the degeneracy of the lowest energy level of the QD exciton originating from the complex valence band structure of the underlying semiconductor material and its splitting by the crystal shape asymmetry, the intrinsic crystal field (in hexagonal lattice structures), and the electron–hole exchange interaction [43]. These effects lead to a fine structure of the hole ground state designated $1S_{3/2}(h)$ (Fig. 3b). Accordingly, the eightfold lowest energy exciton state splits into two groups of closely spaced levels separated by a gap. Some of these states are optically inactive (in the dipole approximation) and are called "dark". The gap between the dark and bright states is observed in the resonantly excited optical emission spectra as a Stokes shift between the lowest absorption maximum and the band-edge emission peak (Fig. 3a). Absorption of a photon by an electronic transition from the highest energy valence band state in such cases is not allowed and is possible only for the optically active state lying deeper in the valence band (see Fig. 3b).

Radiative exciton transitions from the energetically higher excited states (i.e., "bright exciton") are allowed,

---

[1] For clarity, we shall call electron–hole pairs excitons independent of the importance of the Coulomb interaction with repect to the confinement energy.
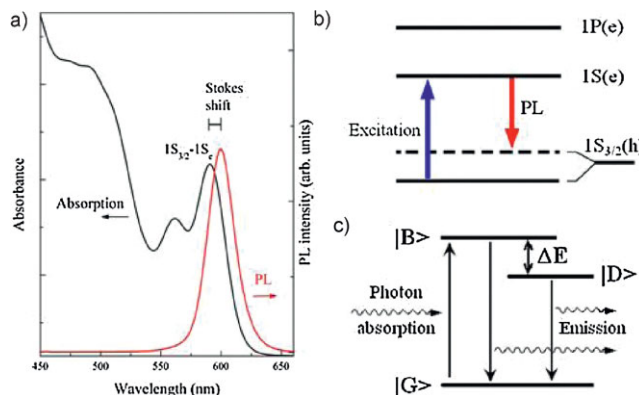
Figure 3 (online color at: www.pss-a.com) (a) PL and absorption spectra of CdSe QDs with mean core diameter of 4.5 nm and a 0.3 nm thick ZnS shell (room temperature). (b) Schematics of the excitation and recombination transitions illustrating separation of the first excited state [1S(e)] from the first optically active state and the optically forbidden (dashed line) ground state. (c) Equivalent representation in terms of exciton recombination. $|G\rangle$ is the ground state; $|B\rangle$ and $|D\rangle$ are the "bright" and "dark" exciton states, respectively.

while those from the lower excited states (i.e., "dark exciton") are dipole forbidden (Fig. 3c). The separation between the "dark" state and the first optically allowed sublevel depends on the QD size [43] and for small dots is much larger than kT, at least at cryogenic temperatures. However, at temperatures above ~ 50 K, phonon-assisted coupling leads to a strong mixing of the "dark" exciton with the optically active states [45]. At room temperature, the value of the Stokes shift can vary between 30 and 150 meV depending on the size and QY of QDs [16]. Also, the net splitting energy resulting from the crystal field and exchange interaction effects (ΔE) is strongly dependent on the size and shape of QDs [43].

From this brief discussion, one can see that the intrinsic electronic structure of a typical nanocrystal QD meets requirement (1) for anti-Stokes cooling. However, it happens that, most likely, the bare exciton level structure described above is not directly related to the PL up-conversion effect. Experimentally, the blue (anti-Stokes) shift between the ASPL peak and E_{abs} does not significantly depend upon the QD size when the excitation photon energy is chosen proportionally to the absorption peak energy (which depends upon the size) [17–26]. This is at variance with the strong size dependence of ΔE. As will be discussed in the next section, a nearly size-independent energy level structure is provided by the interaction with optical phonons in systems with atomic-like bare electronic levels such as QDs.

3.3 Exciton–phonon interaction The importance of phonon effects on the optical properties of semiconductor QD systems has been demonstrated in many works (see reviews [46, 47]). Exciton–phonon coupling in an ideal nanocrystal can be considered in terms of two contributions

resulting from interactions with confined optical and acoustic phonons[2].

The interaction with polar optical phonons can be described as polar Fröhlich coupling of the electric field created by the vibrations of the ionic cores with the Coulomb field of the electron–hole pair. There is also a short-range interaction mechanism via the so-called optical deformation potential (ODP), shown to be quite important for InP nanocrystals [48]. The interaction with acoustic phonons results in a coupling of the electrons and holes to longitudinal acoustic modes via the bulk deformation potential, and to the transverse acoustic modes through the piezoelectric potential.

The Fröhlich coupling of the bulk exciton to longitudinal optical (LO) phonons is usually described in terms of the Huang–Rhys parameter (S), which describes the linewidth and the luminescence Stokes shift with respect to the absorption peak energy

$$\Delta_{\text{Stokes}} = 2S\hbar\omega_{\text{LO}}, \tag{6}$$

where $\hbar\omega_{\text{LO}}$ is the energy of the LO phonon. The S factor is a measure of how strong (large value) or weak (small value) the exciton–phonon coupling is. It can be rigorously defined for a non-degenerate QD exciton state so as to include all the interactions with confined optical phonons [47] and is the only parameter that determines the temperature-dependent exciton spectral function [42]

$$A(E) = 2\pi \exp\left\{-S\left[2\bar{n}(T) + 1\right]\right\} \sum_{n=-\infty}^{+\infty} \left(\frac{\bar{n}(T)+1}{\bar{n}(T)}\right)^{n/2}$$
$$\times I_n\left[2S\sqrt{\bar{n}(T)\left[\bar{n}(T) + 1\right]}\right] \tag{7}$$
$$\times \delta\left(E - E_0 + \Delta - n\hbar\omega_0\right),$$

where $\bar{n}(T)$ is the mean number of the optical phonons at temperature T (given by the Bose–Einstein function), I_n denotes the modified Bessel function, E_0 is the bare exciton energy, $\Delta \approx S\hbar\omega_0$ and $\hbar\omega_0$ is the phonon energy taken the same for all confined modes ($\hbar\omega_0 \approx \hbar\omega_{\text{LO}}$), which is an approximation of the model. The spectral function (7) (often called the Franck–Condon progression) determines both the absorption and emission spectra of the dot (with the replacement $E \to -E$ for the former) and, for large S, peaks at the spectral energy $E = E_0 - \Delta + S\hbar\omega_0$. Since the emission and absorption spectra are the mirror image of each other with respect to the zero-phonon line (ZPL) [42], the shift between their peaks is given approximately by Eq. (6). Note, however, that for a moderate exciton–phonon interaction ($S < 1$) both the emission and absorption spectra are dominated by the ZPL located at $E = E_0 - \Delta$. The interaction with acoustic phonons broadens the discrete energy level structure determined by Eq. (7) and leads to smooth absorption and emission bands that are quite similar

with Lorentzian lineshapes unless the temperature is very low [47].

Using Eq. (6), the exciton–optical-phonon coupling strength can be estimated from the experimental value of the PL Stokes shift under the condition that the position of the PL band is not red shifted by the localization of the exciton by an impurity or surface defects. To this end, large Stokes shifts of excitonic PL band in small II–VI and I–VII QDs have been observed and explained by strong exciton–phonon coupling corresponding to the Huang–Rhys factor values of $S \approx 0.3$ for CdS QDs,[49] $S \approx 1$ for CuBr QDs[50], and larger than unity for CdSe QDs [51, 52].

However, the calculated values of the Huang–Rhys factor are at least one order of magnitude smaller [47, 53]. The experimentally observed strong Stokes shift is probably characteristic of the QD size distribution and not of a single dot and it can be even unrelated to optical phonons (in fact, the Stokes shift can alternatively be explained by the exciton fine structure discussed in the previous section [43]). Because of the limitations of the underlying model and the restricted validity of Eq. (6) ($S \gg 1$), this formula should be used with much care.

There have also been attempts to estimate the value of the Huang–Rhys factor from the ratio between the integrated intensities of the 2LO and LO peaks observed in the resonantly excited Raman spectra [53–57]. Again, quite high values of $S \approx 0.2$–0.5 for CdSe [55, 56], $S \approx 0.7$ for PbS [53], and $S \approx 0.2$–0.7 for CuCl [57]. Possibly the exciton–phonon coupling can be enhanced in real QDs, compared to idealized spherical quantum boxes considered in the calculations due to the separation of the electron and hole resulting from natural variations such as lattice or shape imperfections. This also occurs in core–shell structures [56]. Therefore, the theory can underestimate the value of the Huang–Rhys factor, however, the upper theoretical limit can be obtained by considering a lone electron (i.e., an electron–hole pair completely separated in space). This gives a value of $S \approx 0.3$ for a 2 nm CdSe QD, about 4 times more than for the "ideal" 1S(e)-1S$_{3/2}$(h) exciton [47]. Both the theory [47] and experiment [44, 56] agree that the strength of the electron–phonon coupling increases as the diameter of the QDs is decreased. The high values of the Huang–Rhys factor (as compared to the bulk semiconductors) indicate that the exciton–LO-phonon interactions are quite important in these nanomaterials.

For the sake of completeness, it should be pointed out that for such a strong exciton–phonon coupling, the contribution of non-adiabatic transitions (i.e., the polaron effect) must be important and no single parameter can describe the exciton–polaron spectral function. Consequently, phonon replicas in the PL spectra caused by the recombination of excitons in QDs can disagree with the Franck–Condon progression, both in their spectral positions and relative intensities and the adiabatic approximation (leading to Eq. 7) can be insufficient [58]. Also, it has been shown [59] that the relative intensity ratio between the one-phonon peak and its overtones in the resonant Raman scattering spectra cannot be described by a parameter similar to the Huang–Rhys

---

[2] Strictly speaking, confinement and disorder effects lead to a mixing of the acoustic and optical branches of lattice vibrations.

Phys. Status Solidi A **206**, No. 11 (2009)   2503

Feature
Article

factor. However, these effects are not very important for the qualitative understanding of the phonon-mediated ASPL mechanism in QDs (Section 4) and its application for solid state cooling.

3.4 PL quantum yield of QDs As discussed above, the high PL QY (which is the ratio of the amount of light emitted from a sample to that absorbed by the sample) is required to get net cooling. In this case, non-radiative relaxation of the QD exciton from the excited state that converts the excitation energy into heat will be minimal. Since the QY in semiconductor QDs is determined by the number of surface dangling bonds, inorganic passivation (e.g., CdSe core with a ZnS shell) and/or organic capping ligands can be used to optimize this parameter [16, 60].

At present, commercial CdSe (from Sigma–Aldrich, Invitrogen, Evident, and Plasmachem), CdTe (from Plasmachem), and InP or InGaP (from Evident) QDs are routinely available with a QY of 30–50%. On research side, a series of high quality QDs (such as CdSe and CdTe) with high QY (QY $\approx$ 50–85%) have been successfully prepared by several research groups [16, 61–65]. It has also been shown that post-growth photoetching treatment [36, 66] or QD's growth assisted by microwave irradiation [67] can strongly enhance QY up to an exceptional value of 98% [68], indicating the nearly complete absence of non-radiative decay mechanisms. It is noteworthy that recent studies of QY of QDs at single particle level showed that only a fraction of the QDs in the ensemble are bright. Unlike in dye molecules, the measured QY varies between different individual QDs. A nearly unity single-particle QY has been reported for the brightest sample [41].

Particularly important for cooling device applications is the temperature dependence of QD's QY. Temperature quenching of PL of QDs is a commonly observed phenomenon, both in colloidal suspensions or solvent-free systems such as QDs embedded in polymeric matrices and QD solids, and is ascribed to thermally activated carrier trapping[69, 70]. The greatest QY modification takes place between room temperature and $T \approx 100$ K. Cooling sample down to 100 K temperatures causes approximately fivefold increase in the PL intensity [69] resulting in a QY close to unity even for QD samples with moderate room temperature efficiency [71]. Below this temperature "threshold," the overall PL QY does not change appreciably [71, 72].

3.5 Dependence on the excitation wavelength and ASPL efficiency It is commonly accepted that the emission wavelength and emission efficiency of QDs are independent [69] (or almost independent [73]) of the excitation wavelength when the excitation is provided above the first absorption maximum. However, by tuning the excitation wavelength to the red edge of the QD absorption peak, the effect of the inhomogeneous broadening caused by the distribution of QD sizes can lead to strong PL line
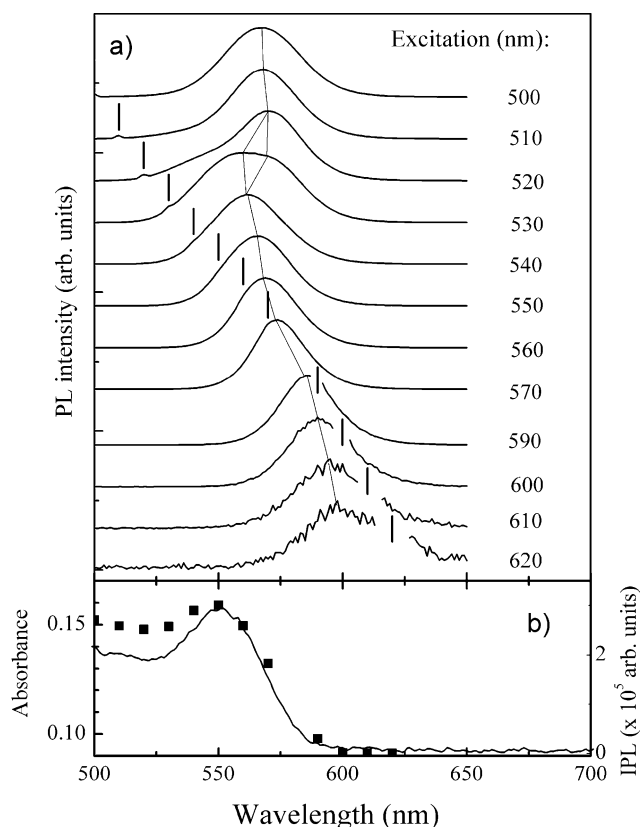
Figure 4 (a) PL spectra of CdSe/ZnS QDs in toluene for various excitation wavelengths at room temperature. For each spectrum the excitation energy is marked by the vertical bars. All PL spectra are normalized for comparison. (b) The absorption spectrum of the sample. Black squares indicate the IPL values for various excitation wavelengths.

narrowing and spectral shifts since only the largest QDs in the sample will be excited [74, 75].

Figure 4a shows PL spectra of 4 nm size CdSe/ZnS QDs measured at room temperature. They were recorded by varying the excitation wavelength (λ_{exc}) from 500 to 620 nm, i.e., from the high energy region of the absorption spectrum to the tail far below the first absorption peak (Fig. 4b). When the excitation is provided between 500 and 520 nm, the position of the Stokes-shifted emission peak is almost independent of λ_{exc}. For this sample, the value of the "non-resonant Stokes shift" (i.e., the difference between the lowest-energy peak in the absorption spectra and the emission peak) is about 67 meV. The PL linewidth shows only a very small additional broadening with an increase in the excitation energy in this region. This weak dependence of the linewidth and the non-resonant Stokes shift is due to the fact that for a higher excitation energy the PL spectrum better reflects the entire size distribution of QDs in the sample. While the data presented in Fig. 4a are normalized for comparison, in the absolute scale, a 7% reduction of the integrated PL intensity (IPL) has been observed as λ_{exc} decreases from 500 to 520 nm (Fig. 4b).

Providing excitation between 520 and 540 nm, the emission profile becomes more complex. A weak shoulder appears on the blue edge of PL band as λ_{exc} increases up to 520 nm. For higher excitation wavelength (530 nm), the PL spectrum has one very broadband, which can be deconvoluted into two peaks. This double peak structure can be explained as a result of size-selective excitation within the population of QDs and is expected for an inhomogeneously broadened system. Since there are multiple states present in each dot, there is a region of λ_{exc} (520–530 nm for the present sample) where the largest QDs can be excited into their second excited state, while smaller size dots are excited into their first excited state. Since each nanocrystal emits primarily at a certain photon energy (corresponding to its exciton ZPL), regardless of the excitation wavelength, at this point the emission spectrum shows two peaks, one from the set of smaller particles absorbing into their first state and the second from the larger QDs excited into their second state [74].

As the excitation wavelength is tuned further below the first absorption maximum of 550 up to 570 nm, one PL peak is observed again, whose emission energy shifts to the red with increasing λ_{exc}. The width of the PL peak decreases considerably in this spectral region (from ∼31 nm at λ_{exc} = 540 nm to ∼20 nm at λ_{exc} = 570 nm) demonstrating the PL line narrowing. This is because only larger QDs within the finite size distribution are excited on the low energy side of the absorption profile. On the other hand, a 52% reduction in the IPL intensity has been observed as the excitation energy decreases in this spectral region because only a very small fraction of the QD size distribution is selected to be excited.

A distinctly different behavior is observed in the spectral region far below the absorption peak (Fig. 4a). A tail of ASPL can be seen with 590 nm excitation, ranging up to 40 nm below λ_{exc}. A similar decaying anti-Stokes tail in PL has been also observed in InP [23] and CdTe [76] QDs. At still higher excitation wavelength, a pronounced ASPL peak appears, which shifts to the red following the excitation wavelength. Actually, the progressive transition from SSPL into ASPL is evident in Fig. 4a, λ_{exc} > 590 nm. A similar observation was reported recently for PbS QDs [25]. The gradual change in the band shape suggests that the physical process involved in the QD emission is the same throughout the whole range of excitation energies. However, in contrast to SSPL, the ASPL does not reflect the entire size distribution of the QDs. As mentioned above, the effect of inhomogeneous broadening caused by the distribution of QDs sizes can be clearly seen in the excitation wavelength dependence of the SSPL spectra (Fig. 2a, λ_{exc} region 520–530 nm). When the excitation is restricted to the onset region of the absorption spectra, then QDs of a much narrower size range are excited; these QDs are the largest in the ensemble. In this spectral region the SSPL spectra of QDs show a decrease of the width of the PL band demonstrating the pronounced line narrowing. In contrast, the ASPL linewidth shows extra broadening with the increasing of the excitation wavelength, from 22 nm at λ_{exc} = 590 nm to 40 nm at λ_{exc} = 620 nm.

In terms of the optical cooling process it is important that the rate constants of non-radiative relaxation of the first excited state are independent of the method of excitation within the absorption band (the Stokes-shifted PL) or at its long-wavelength edge (the anti-Stokes PL), that is, the QY of the Stokes PL is equal to that of the anti-Stokes PL. Time-resolved PL studies of QDs in the anti-Stokes regime are scarce [22] and do not provide data on the ASPL decay time. However, the data presented in Fig. 4b strongly suggest that the IPL intensity plotted *versus* the excitation wavelength reproduces with high accuracy the absorption spectra of QDs. The good correspondence obtained between the spectral positions of the absorption and anti-Stokes IPL peaks implies that the origin of the observed ASPL band is the radiative recombination of the excitons confined in the dots.

It is noteworthy that all spectra presented in Fig. 4a were obtained by exciting the samples with a Xenon lamp (output power of 40 μW–0.1 mW, depending on the spectral region). This demonstrates that the (phonon-assisted) excitation of the ASPL in QDs is a highly efficient process, since even for samples with moderate QY (≈20%) there is no need for laser excitation. Also it can be seen that the ASPL efficiency is comparable with that of SSPL, at least for small magnitudes of the up-converted blue shift ΔE (e.g., at λ_{exc} = 590 nm for the present sample).

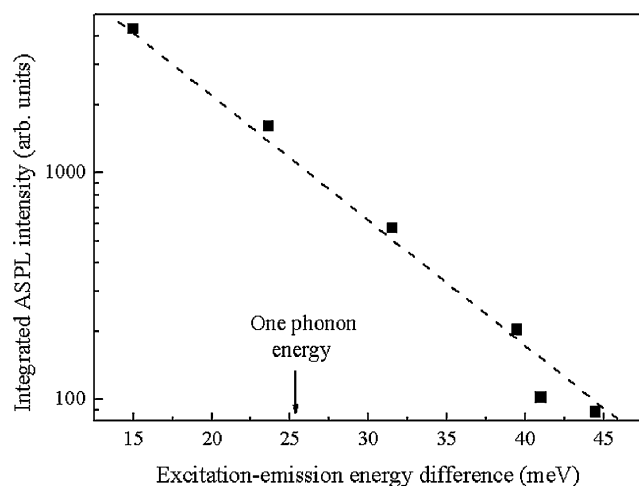**3.6 ASPL dependence on temperature and excitation power** As has been mentioned above, the ASPL intensity increases strongly with temperature. Indeed, this behavior was reported for CdSe[20, 23], and CdTe [20, 22, 77] QDs. An increase of up to 12 times in the ASPL intensity was achieved for CdSe QDs when the sample was heated in the temperature range 283–353 K. [78]. Thus, the ASPL process occurs as a result of the thermally activated up-conversion of the optically created exciton in the dot. It turns out that the thermally stimulated increase in the ASPL is almost independent of the size of the QDs, although it is more efficient in QDs with higher QY [17, 19]. The spectral position of the ASPL peak showed little dependence on temperature, whereas the variation of the peak energy of the SSPL band was found to be considerable and practically coincident with that of the absorption peak energy corresponding to the $1S(e) \rightarrow 1S_{3/2}(h)$ transition [17, 19]. As we will be discussed in Section 4, these experimental findings demonstrate the key role of the exciton–phonon interaction in the ASPL process in QDs.

As is known [23, 79] the analysis of the dependence of the ASPL intensity on the excitation intensity (I_{exc}) usually can give information on the mechanism of energy transfer in the high energy spectral region. Thus, for two-photon excitation or two-stage excitation of electrons from the valence to the conduction band through deep impurity levels, a quadratic dependence, $I_{ASPL} \propto I_{exc}^2$, should be observed [79]. For an ASPL process induced by Auger recombination, a cubic dependence, $I_{ASPL} \propto I_{exc}^3$, is characteristic [80], whereas in

Phys. Status Solidi A **206**, No. 11 (2009)　　　　　　　　　　　　　　　　　　　　2505

Feature
Article

the case of mixed mechanisms, the power-law dependence of I_{ASPL} on I_{exc} becomes more complicated [81].

In light of the above model for the exciton population densities at equilibrium established by phonon absorption/emission (Fig. 1a), the photon energy up-conversion involved in the optical cooling is a linear process in terms of the excitation intensity. The linear proportionality between I_{ASPL} (or I_2 in Eq. (2)) and I_{exc} has been verified experimentally for various QD materials, with a slope depending on the QY of the sample [18, 20, 22, 23, 77]. However, when analyzing an up-converted PL signal, the linear dependence of the ASPL intensity on I_{exc} alone cannot be taken as an indication of the participation of phonons in the excitation process. The same dependence can be observed, for example, for two-photon or two-step excitation under conditions of saturation.[21] A credible conclusion for the mechanisms of ASPL must be supported by a series of independent measurements. In this respect, studies of the temperature dependence of the anti-Stokes PL are the most conclusive especially when combined with the results of the excitation-selective PL spectroscopy.

Figure 5 shows the anti-Stokes efficiency of QDs plotted as a function of the difference in energy between the excitation and ASPL band maximum (equivalent to ΔE in Fig. 1a). It shows that an exponential dependence fits experimental points quite well. One can see that the energy mismatch ΔE is larger than 26 meV, the LO phonon energy in CdSe. This fact, together with the exponential functional form of the probability for anti-Stokes excitation with respect to ΔE, further demonstrate that we are dealing with phonon-assisted excitation. This picture shows also that ASPL excitation is still possible at ΔE bigger than 45 meV at room temperature and ΔE can reach some 150 meV.[20] As discussed in the next section, such a hi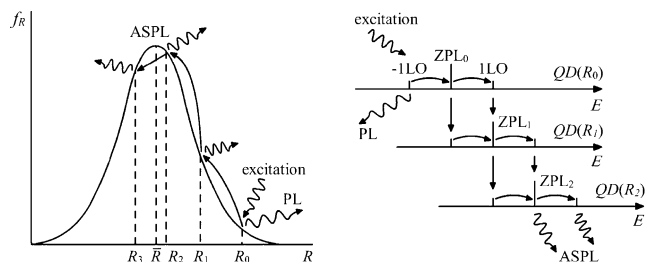gh anti-Stokes shift is possible due to several up-conversion events taking place through in different QDs within the sample that are consecutively excited through photon re-absorption. The pseudo-continuous distribution of dot sizes provides the appropriate exciton energy spectrum of the QD ensemble where the approximately exponential decreasing dependence of the up-conversion probability on ΔE is verified at a fixed temperature (Fig. 5).

4 Mechanism of anti-Stokes PL in nanocrystal quantum dots

4.1 Phonon-assisted up-conversion in a single QDs As has been discussed in Section 3.3, the energy spectrum of excitons in QDs is strongly modified due to the interaction with optical phonons that is enhanced compared to bulk semiconductors because of the electron, hole, and phonon confinement [47]. The true stationary states of the interacting system consisting of an exciton and phonons are called exciton–polaron states, which have been observed experimentally in nanocrystal QDs by using size-selective PL [82] and pump-and-probe transmission [49] spectroscopy. In the simplest model case of just one "bare" exciton level, the exciton–polaron spectral function is given by Eq. (7). It was suggested [58, 83] that the polaron absorption peaks lying beneath the exciton ground energy level (e.g., the "−1LO" satellite, see Fig. 6, right panel) can be responsible for the excitation of QDs below the inter-band absorption limit. For realistic values of the exciton–phonon coupling parameter ($S \approx 0.1$–0.2), only the ZPL and its first satellites ("−1LO" and "1LO") are really important. After absorbing a photon and reaching thermal equilibrium, the excited dot can emit a photon, most likely with the energy corresponding to the ZPL or (more rarely) with that corresponding to the "1LO" satellite in the emission spectrum. The energy gain of $\hbar\omega_0$ or $2\hbar\omega_0$, respectively, comes from the thermostat that maintains the dot at a given temperature. This explains why

Figure 5 Dependence of the integrated ASPL intensity on the excitation–emission energy difference in CdSe/ZnS nanocrystals at room temperature.

Figure 6 Cascade energy transfer process in an ensemble of QDs with the radius distribution shown in the left panel. A large dot, of radius R_0, is excited through its "-1LO" absorption peak and emits through either ZPL or "1LO" satellite, with an up-conversion equal to $\hbar\omega_0$ or $2\hbar\omega_0$, respectively. The emitted photon eventually is re-absorbed by a smaller dot, of radius R_1, and then re-emitted, in some cases with a higher energy. At each step, some photons leave the sample while some are re-absorbed by still smaller QDs. The process repeats until the number of dots of the appropriate size, able to re-absorb the photon becomes too small. (Reproduced from Ref. [84] with permission of the American Physical Society.)

the anti-Stokes shift (i.e., the gap between the absorbing and emitting states) does not depend on the QD radius (R), because the energy of confined optical phonons changes only very weakly with R [47]. The strongly increasing temperature dependence of the ASPL intensity is naturally explained by the raising of the satellite peaks in both absorption and emission (roughly, proportional to the Bose–Einstein function for the LO phonon) [58].

Indeed, since the thermally activated ASPL has been observed for several different types of NCs, the intermediate states involved in the mechanism must be intrinsic to QDs, independently of their material and covering shell. The exciton–polaron states appear as natural candidates for this role. However, it seems to be difficult to explain the observed values of the up-converted shift which are much larger than the LO phonon energy. Of course, there are "-nLO" and "nLO" satellites with $n > 1$ in the QD spectra, but their intensities are much too low for realistic values of the electron–phonon coupling constants [47]. A clue to the understanding of the large anti-Stokes shift is the experimentally established fact that the ASPL can occur only in samples with a sufficiently long optical pathway, implying that it is a result of several consecutive up-conversion events occurring in different QDs within the sample [84].

4.2 Cascade up-conversion in a QD ensemble
If the optical density of the sample is high enough, re-absorption and re-emission of photons by different QDs within it are possible and the spectral shift is larger than can be explained by a cascade excitation process as schematically shown in Fig. 6. The ASPL process is initiated through the excitation of one of the largest (and rare) dots in the ensemble. In some cases, the emission occurs at a higher energy and such a photon has a larger chance to be re-absorbed because there are more dots of the appropriate size. Both the up-converted emission and re-absorption processes are enhanced with temperature, since the corresponding cross-sections are both proportional to the spectral function (7)

$$\sigma_a(E) \propto A(E);$$
$$\sigma_e(E) \propto \exp\left(\frac{-E}{kT}\right) A(E). \tag{8}$$

The probability of the re-absorption of a photon of energy E (up-converted in the first dot), per unit time is given by

$$P_1 = N\frac{c}{n}\left[\sigma_a^{(-1)}(E+\hbar\omega_0)f(E+\hbar\omega_0) + \sigma_a^{(0)}(E)f(E)\right.$$
$$\left. + \sigma_a^{(+1)}(E-\hbar\omega_0)f(E-\hbar\omega_0)\right], \tag{9}$$

where N is the overall concentration of NCs, c is the velocity of light, n is the refraction index of the medium where the NCs are embedded, $\sigma_a^{(j)}$ is the absorption cross-section of the jLO satellite peak (Eqs. 7 and 8), and f denotes the distribution function of the bare exciton energies in the dot. The latter is determined by the QD radius distribution
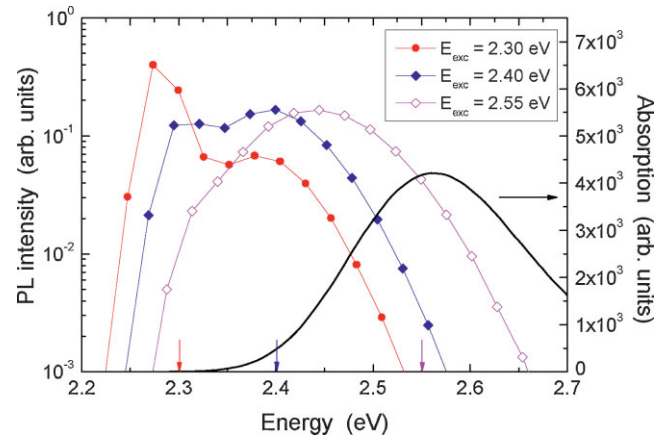
Figure 7 (online color at: www.pss-a.com) Calculated room temperature emission and absorption spectra of a colloidal solution of CdSe QDs. The emission spectra were calculated for three different values of the incident photon energy using a Monte-Carlo procedure. The QD radius distribution function was taken as Gaussian with $\langle R \rangle$ and a standard deviation of 5%. The absorption spectrum was calculated using the effective mass approximation. (Reproduced from Ref. [84] with permission of the American Physical Society.)

function, shown schematically in Fig. 6, since E and R are related (the widely used relation obtained within the effective-mass approximation can be found, e.g., in Refs. [43, 47]). According to Eq. (9), QDs of three different sizes can re-absorb the photon and two of these three possibilities can lead to up-conversion (Fig. 6).

After the re-absorption in a dot of size R_1, again, there are two channels for further up-conversion, with the probabilities proportional to the corresponding terms in $\sigma_e(E)$ (Eqs. (7) and (8)). Then similar re-absorption processes can take place for the (secondary) re-emitted photon, etc.

Of course, many of the emitted photons just leave the sample contributing to the unshifted or slightly shifted luminescence, which is always observed along with the up-converted component. The cascade re-absorption/re-emission process continues until the number of dots in the sample that are able to re-absorb becomes too small. Then, beyond the usual (unshifted) luminescence, a spectral maximum is formed at a higher frequency. The results of the Monte-Carlo modeling of the processes illustrated in Fig. 6 and described by Eqs. (7)–(9), performed in Ref. [84] show that, in accordance with the experimental data, the observation of the ASPL requires the appropriate choice of the excitation wavelength (see Fig. 7) and high optical density of the QD solution. It also confirms the principal experimental findings summarized above.

5 Feasibility of the anti-Stokes cooling with nanocrystal QDs
Most of the practical applications of semiconductor colloidal QDs are based on nanocrystal ensembles incorporated into a variety of host materials, such as organic or inorganic solvents, glass, or polymer films.

Phys. Status Solidi A **206**, No. 11 (2009)

2507

Feature
Article

However, the highest QY value that has been reported to date is for QDs colloidal solutions in organic solvents and we will focus on this case using some of the experimental data discussed above. The presence of the host material implies that, in terms of the anti-Stokes optical cooling, the absorption of excitation light by both QDs themselves and by the solvent must be taken into account. Also, the distribution of QD sizes results in the corresponding distribution of the emission wavelength, λ_{PL}. The cooling model described in Section 2 can be modified in order to take these effects into account [85] by rewriting Eq. (4) in terms of cooling power as

$$P_{cool} = \left(\eta_q \frac{\lambda_{abs}}{\lambda^*} A_{QD} - A_{comp} \right) P_{ex}, \tag{10}$$

where P_{ex} is the PL excitation power, λ_{abs} corresponds to the wavelength of excitation (λ_{exc}), A_{QD} is the absorbance of QDs themselves, A_{comp} is the absorbance of the composite QDs and host material (both at λ_{exc}), and λ^* is the mean wavelength of the fluorescence given by

$$\lambda^* = \frac{\int F(\lambda) d\lambda}{\int (1/\lambda) F(\lambda) d\lambda}, \tag{11}$$

where $F(\lambda)$ is the PL energy spectrum.

In Eq. (10) the host absorbance (A_{comp}) also takes into account both the intrinsic solvent absorption and the absorption due to impurities. The absorption due to such non-luminescent components can be described by a quantity A_{nl}. For small values of A_{QD} and A_{nl}, we have $A_{comp} = A_{QD} + A_{nl}$ and one obtains from Eq. (10) the following expression for the net cooling power

$$P_{cool} = \left[\eta_q \frac{\lambda_{abs}}{\lambda^*} - \left(1 + \frac{A_{nl}}{A_{QD}} \right) \right] P_{ex} A_{QD}. \tag{12}$$

Obviously, the anti-Stokes cooling take place if $P_{cool} > 0$. Then the threshold QY value (above which the cooling is possible) can be derived from Eq. (12)

$$\eta_{th} = \frac{\lambda^*}{\lambda_{abs}} \left(1 + \frac{A_{nl}}{A_{QD}} \right). \tag{13}$$

As discussed in Sections 3 and 4, the ASPL efficiency in QDs strongly depends on excitation wavelength (Figs. 4b and 5). Using these experimental data and Eq. (13), we can calculate the spectral distribution of η_{th} values for our CdSe/ZnS QDs in toluene. As one can see from Fig. 4, λ^* of the ASPL band of QDs depends on the excitation wavelength and has to be estimated using Eq. (11).

The data for $A_{nl} = 0$ in Fig. 8 represent an ideal case where no excitation energy is dissipated by the host absorption. Even in this case, QY as high as 0.965 is required to provide anti-Stokes cooling with excitation at 620 nm when the
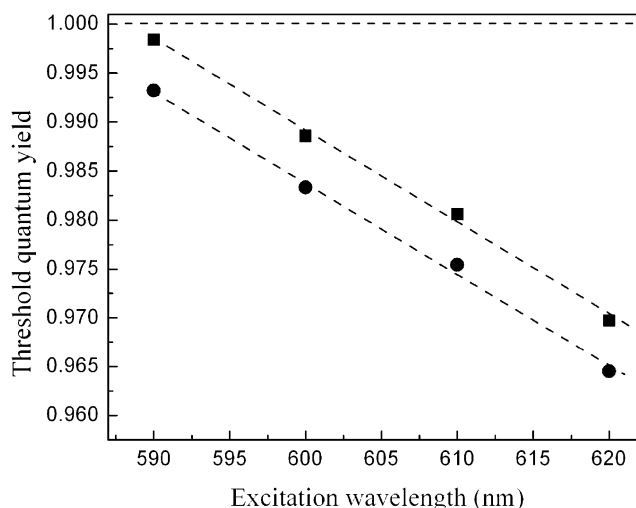
Figure 8 Threshold QY (η_{th}) value *versus* excitation wavelength λ_{exc} for CdSe QDs in toluene calculated for $A_{nl} = 0$ (circles) and $A_{nl} = 5 \times 10^{-4}$ (squares). The horizontal dashed line represents level of QY = 100%.

difference between the excitation and emission wavelengths (and, therefore, the cooling efficiency is a maximum (see Fig. 4a and Eq. (5)). In practice, the absorption by the host material cannot be neglected. Even the very small absorption of toluene (spectroscopy grade) of 5×10^{-4} raises the value of η_{th} (Fig. 8). Such a high value of QDs QY is still a challenge at present [68]. Extrapolating the data in Fig. 8 by a linear function we can predict that the excitation wavelength has to be at least 700 nm to provide efficient cooling with QDs of 0.85 QY, which can be more or less routinely achieved [64, 65]. It is noteworthy, however, that at this wavelength the excitation of ASPL in CdSe/ZnS QDs samples discussed here, is highly inefficient (see Fig. 4). Since the ASPL efficiency depends linearly on the pump power, a rather obvious solution is to increase the excitation level. However, at high excitation intensity a number of undesirable side effects come into play, such as photodegradation of the sample. Also, radiative or non-radiative nonlinear effects like two-photon absorption or Auger recombination, respectively, can strongly reduce the efficiency of ASPL and therefore, the cooling efficiency.

Several means can be suggested in order to enhance the QY of the QDs or to eliminate unwanted nonlinear effects. One of the possible approaches is metal-enhanced fluorescence, a newly recognized technology where the interactions of the light emitter with metallic colloids or surfaces provides efficient PL enhancement. In the coupling process, the energy of the light emitter can be transferred into surface plasmon modes of the metal nanostructures and then radiated in such a way that the effective emission efficiency is enhanced. A significant (up to fivefold) enhancement in the PL intensity was recently reported for the CdSe-ZnS/polyelectrolyte/Au nanostructure [86] and for CdTe QDs deposited on the silver nano-island

films [87]. Theoretical analysis shows that the threshold and the efficiency of laser cooling can be significantly improved due to energy transfer from semiconductor to metal [88].

It has been recently realized that careful band-gap engineering of semiconductor QDs can provide core–shell nanostructures for which nonlinear Auger recombination is simply inactive [89]. One such approach, which involved the use of type-II core/shell hetero-QDs, was recently demonstrated in Ref. [90]. Spatial separation of electrons and holes in these nanostructures produces a significant imbalance between negative and positive charges, which results in a strong local electric field. This field spectrally displaces the absorbing transition in excited QDs with respect to the emission line via the carrier-induced Stark effect. Moreover, this also should increase the exciton–phonon coupling and therefore the ASPL efficiency [84]. Although there are no reports to date on ASPL in such QDs, these studies might open the way for anti-Stokes cooling at high pump powers.

Finally, perhaps the simplest solution to the problem of insufficient QY of QDs is to decrease the dot temperature by one of the conventional methods. Cooling the sample down to ∼100 K results in the QY close to unity (Section 3.4). To this end, the most feasible concept for QDs anti-Stokes cooling is combined in a Peltier and optical cooling device, when first the sample is cooled down to the threshold QY by thermoelectric cooling and then phonon-assisted optical cooling takes over.

To conclude, recent experimental results demonstrate that all the requirements for optical cooling using semiconductor colloidal QDs, outlined in Section 3.3 can be met. The appropriate electronic structure, strong electron–phonon interaction, high quantum efficiency of PL, and the efficient thermally stimulated anti-Stokes PL in QDs are the conditions that are highly favorable for the first observation of anti-Stokes cooling. The rapid development of new nano-technological tools and techniques in this field ensures that answering the question about the feasibility of optical cooling with QDs one can say "when" rather than "if".

References

[1] P. Pringsheim, Z. Phys. **57**, 739 (1929).
[2] T. W. Hänsch and A. L. Schawlow, Opt. Commun. **13**, 68 (1975).
[3] E. H. Kennard, Phys. Rev. **29**, 466 (1927).
[4] R. W. Wood, Philos. Mag. **6**, 310 (1928).
[5] L. Landau, J. Phys. **10**, 503 (1946).
[6] R. I. Epstein, M. I. Buchwald, B. C. Edwards, T. R. Gosnell, and C. E. Mungan, Nature **377**, 500 (1995).
[7] C. E. Mungan, M. I. Buchwald, B. C. Edwards, R. I. Epstein, and T. R. Gosnell, Phys. Rev. Lett. **78**, 1030 (1997).
[8] J. L. Clark and G. Rumbles, Phys. Rev. Lett. **76**, 2037 (1996).
[9] C. W. Hoyt, M. Sheik-Bahae, R. I. Epstein, B. C. Edwards, and J. E. Anderson, Phys. Rev. Lett. **87**, 3600 (2000).
[10] M. Sheik-Bahae and R. I. Epstein, Phys. Rev. Lett. **92**, 247403 (2004).
[11] B. Imangholi, M. P. Hasselbeck, R. I. Epstein, and S. Kurtz, Proc. SPIE **6115**, 611518 (2006).
[12] M. Sheik-Bahae and R. I. Epstein, Nature Photonics **1**, 693 (2007).
[13] E. Finkeissen, M. Potemski, P. Wyder, L. Vina, and G. Wiemann, Appl. Phys. Lett. **75**, 1258 (1999).
[14] G. C. Dousmanis, C. W. Mueller, H. Nelson, and K. G. Petzinger, Phys. Rev. **133**, A316 (1964).
[15] J. Yao, D. R. Larson, H. D. Vishwasrao, W. R. Zipfel, and W. W. Webb, Proc. Natl. Acad. Sci. USA **102**, 14284 (2005).
[16] A. L. Rogach, T. Franzl, T. A. Klar, J. Feldmann, N. Gaponik, V. Lesnyak, A. Shavel, A. Eychmüller, Y. P. Rakovich, and J. F. Donegan, J. Phys. Chem. C **111**, 14628 (2007).
[17] K. I. Rusakov, A. A. Gladyshchuk, Y. P. Rakovich, J. F. Donegan, S. A. Filonovich, M. J. M. Gomes, D. V. Talapin, A. L. Rogach, and A. Eychmüller, Opt. Spectrosc. **94**, 921 (2003).
[18] Y. P. Rakovich, J. F. Donegan, S. A. Filonovich, M. J. M. Gomes, D. V. Talapin, A. L. Rogach, and A. Eychmüller, Phys. E **17**, 99 (2003).
[19] S. A. Filonovich, M. J. M. Gomes, Y. P. Rakovich, J. F. Donegan, D. V. Talapin, N. P. Gaponik, A. L. Rogach, and A. Eychmüller, MRS Proc. **737**, 157 (2003).
[20] Y. P. Rakovich, S. A. Filonovich, M. J. M. Gomes, J. F. Donegan, D. V. Talapin, A. L. Rogach, and A. Eychmüller, Phys. Status Solidi B **229**, 449 (2002).
[21] A. G. Joly, W. Chen, D. E. McCready, J.-O. Malm, and J.-O. Bovin, Phys. Rev. B **71**, 165304 (2005).
[22] X. Wang, W. W. Yu, J. Zhang, J. Aldana, X. Peng, and M. Xiao, Phys. Rev. B **68**, 125318 (2003).
[23] E. Poles, D. C. Selmarten, O. I. Micic, and A. J. Nozik, Appl. Phys. Lett. **75**, 971 (1999).
[24] W. Chen, J. Chem. Phys. **122**, 224708 (2005).
[25] M. J. Fernee, P. Jensen, and H. Rubinsztein-Dunlop, Appl. Phys. Lett. **91**, 043112 (2007).
[26] J. M. Harbold and F. W. Wise, Phys. Rev. B **76**, 125304 (2007).
[27] V. Colvin, M. Schlamp, and A. Alivisatos, Nature **370**, 354 (1994).
[28] M. Y. Gao, C. Lesser, S. Kirstein, H. Mohwald, A. L. Rogach, and H. Weller, J. Appl. Phys. **87**, 2297 (2000).
[29] S. V. Kershaw, M. T. Harrison, and M. G. Burt, Philos. Trans. **361**, 331 (2003).
[30] Y. P. Rakovich, J. F. Donegan, M. Gerlach, A. L. Bradley, T. M. Connolly, J. J. Boland, N. Gaponik, and A. Rogach, Phys. Rev. A **70**, 051801 (2004).
[31] Y. P. Rakovich, L. Yang, E. M. McCabe, J. F. Donegan, T. Perova, A. Moore, N. Gaponik, and A. Rogach, Semicond. Sci. Technol. **18**, 914 (2003).
[32] A. S. Susha, F. Caruso, A. L. Rogach, G. B. Sukhorukov, A. Kornowski, H. Möhwald, M. Giersig, A. Eychmüller, and H. Weller, Colloids Surf. A **163**, 39 (2000).
[33] A. P. Alivisatos, W. Weiwei Gu, and C. Larabell, Annu. Rev. Biomed. Eng. **7**, 55 (2005).
[34] I. Nabiev, S. Mitchell, A. Davies, Y. Williams, D. Kelleher, Y. K. Gun'ko, S. Byrne, Y. P. Rakovich, J. F. Donegan, A. Sukhanova, D. Cottell, N. Gaponik, A. Rogach, and Y. Volkov, Nano Lett. **7**, 3452 (2007).

Phys. Status Solidi A **206**, No. 11 (2009)

Feature

Article

2509

[35] L. Brus, J. Phys. Chem. Solids **59**, 459 (1998).
[36] B. Rossi, H. J. Byrne, W. Blau, P. Pratesi, and S. Sottini, J. Opt. Soc. Am. B **8**, 2449 (1991).
[37] C. E. Mungan and T. R. Gosnell, Laser Cooling of Solids, in: Advances in Atomic, Molecular and Optical Physics, edited by B. Bederson and H. Walther (Academic Press, San Diego, 1999), pp. 161–227.
[38] M. A. Weinstein, J. Opt. Soc. Am. **50**, 597 (1960).
[39] S. Vavilov, J. Phys. **9**, 68 (1945).
[40] S. Vavilov, J. Phys. **10**, 499 (1946).
[41] Y. Ebenstein, T. Mokari, and U. Banin, Appl. Phys. Lett. **80**, 4033 (2002).
[42] S. Schmitt-Rink, D. A. B. Miller, and D. S. Chemla, Phys. Rev. B **35**, 8113 (1987).
[43] Al. L. Efros, M. Rosen, M. Kuno, M. Nirmal, D. J. Norris, and M. Bawendi, Phys. Rev. B **54**, 4843 (1996).
[44] M. Nirmal, D. J. Norris, M. Kuno, M. G. Bawendi, Al. L. Efros, and M. Rosen, Phys. Rev. Lett. **75**, 3728 (1995).
[45] S. Xu, A. A. Mikhailovsky, J. J. Hollingsworth, and V. I. Klimov, Phys. Rev. B **65**, 045319 (2002).
[46] A. Uhrig, A. Worner, C. Klingshirn, L. Banyai, S. Gaponenko, I. Lacis, N. Neuroth, B. Speit, and K. Remitz, J. Cryst. Growth **117**, 598 (1992).
[47] M. I. Vasilevskiy, Exciton-phonon interaction in semiconductor nanocrystals, in: Semiconductor Nanocrystal Quantum Dots, edited by A. L. Rogach (Springer, New York, 2008), pp. 217–255.
[48] A. G. Rolo, M. I. Vasilevskiy, M. Hamma, and C. Trallero-Giner, Phys. Rev. B **78**, 081304 (2008).
[49] U. Woggon, M. Saleh, A. Uhrig, M. Portune, and C. Klingshirn, J. Cryst. Growth **138**, 988 (1994).
[50] J. Valenta, J. Moniatte, P. Gilliot, B. Hönerlage, J. B. Grun, R. Levy, and A. I. Ekimov, Phys. Rev. B **57**, 1774 (1998).
[51] V. Jungnickel and F. Henneberger, J. Lumin. **70**, 238 (1996).
[52] S. A. Empedocles, D. J. Norris, and M. G. Bawendi, Phys. Rev. Lett. **77**, 3873 (1996).
[53] T. D. Krauss and F. W. Wise, Phys. Rev. B **55**, 9860 (1997).
[54] A. P. Alivisatos, T. D. Harris, P. J. Carroll, M. L. Steigerwald, and L. E. Brus, J. Chem. Phys. **90**, 3463 (1989).
[55] M. C. Klein, F. Hache, D. Ricard, and C. Flytzanis, Phys. Rev. B **42**, 11123 (1990).
[56] A. V. Baranov, Y. P. Rakovich, J. F. Donegan, T. S. Perova, R. A. Moore, D. V. Talapin, A. L. Rogach, Y. Masumoto, and I. Nabiev, Phys. Rev. B **68**, 165306 (2003).
[57] A. V. Baranov, S. Yamauchi, and Y. Masumoto, Phys. Rev. B **56**, 10332 (1997).
[58] M. I. Vasilevskiy, E. V. Anda, and S. S. Makler, Phys. Rev. B **70**, 035318 (2004).
[59] R. P. Miranda, M. I. Vasilevskiy, and C. Trallero-Giner, Phys. Rev. B **74**, 115317 (2006).
[60] B. O. Dabbousi, J. Rodriguez-Viejo, F. V. Mikulec, J. R. Heine, H. Mattoussi, R. Ober, K. F. Jensen, and M. G. Bawendi, J. Phys. Chem. B **101**, 9463 (1997).
[61] Z. A. Peng and X. Peng, J. Am. Chem. Soc. **123**, 183 (2001).
[62] D. V. Talapin, A. L. Rogach, A. Kornowski, M. Haase, and H. Weller, Nano Lett. **1**, 207 (2001).
[63] T. C. Kippeny, M. J. Bowers, A. D. Dukes, J. R. McBride, R. L. Orndorff, M. D. Garrett, and S. J. Rosenthal, J. Chem. Phys. **128**, 084713 (2008).
[64] C. de Mello Donega, S. G. Hickey, S. F. Wuister, D. Vanmaekelbergh, and A. Meijerink, Phys. Chem. B **107**, 489 (2003).
[65] P. Reiss, S. Carayon, and J. Bleuse, Phys. E **17**, 95 (2003).
[66] N. Gaponik, D. V. Talapin, A. L. Rogach, K. Hoppe, E. V. Shevchenko, A. Kornowski, A. Eychmuller, and H. Weller, J. Phys. Chem. B **106**, 7177 (2002).
[67] Y. He, H. T. Lu, L. M. Sai, W. Y. Lai, Q. L. Fan, L. H. Wang, and W. Huang, J. Phys. Chem. B **110**, 13370 (2006).
[68] Y. He, L.-M. Sai, H.-T. Lu, M. Hu, W.-Y. Lai, Q.-L. Fan, L.-H. Wang, and W. Huang, Chem. Mater. **19**, 359 (2007).
[69] G. W. Walker, V. C. Sundar, C. M. Rudzinski, A. W. Wun, M. G. Bawendi, and D. G. Nocera, Appl. Phys. Lett. **83**, 3555 (2003).
[70] S. A. Crooker, T. Barrick, J. A. Hollingsworth, and V. I. Klimov, Appl. Phys. Lett. **82**, 2793 (2003).
[71] Y. Nonoguchi, T. Nakashima, and T. Kawai, J. Phys. Chem. C **112**, 19263 (2008).
[72] D. Valerini, A. Cretí, M. Lomascolo, L. Manna, R. Cingolani, and A. Anni, Phys. Rev. B **71**, 235409 (2005).
[73] M. Hosokawa, Development of bright phospors using glasses incorporating semiconductor nanoparticles, in: Nanoparticle Technology Handbook (Elsevier, Oxford, 2007), p. 558.
[74] W. Hoheisel, V. L. Colvin, C. S. Johnson, and A. P. Alivisatos, J. Chem. Phys. **101**, 8455 (1994).
[75] O. I. Micic, H. M. Cheong, H. Fu, A. Zunger, J. R. Sprague, A. Mascarenhas, and J. Nozik, J. Phys. Chem. B **101**, 4904 (1997).
[76] D. V. Talapin, S. Haubold, A. L. Rogach, A. Kornowski, M. Haase, and H. Weller, J. Phys. Chem. B **105**, 2260 (2001).
[77] Y. P. Rakovich, A. A. Gladyshchuk, K. I. Rusakov, S. A. Filonovich, M. J. M. Gomes, D. V. Talapin, A. L. Rogach, and A. Eychmüller, J. Appl. Spectrosc. **69**, 444 (2002).
[78] Y. P. Rakovich, J. F. Donegan, S. A. Filonovich, M. J. M. Gomes, D. V. Talapin, A. L. Rogach, and A. Eychmüller, in: Proceedings of the 26th International Conference on the Physics of Semiconductors, Edinburgh, UK, 2003, Institute of Physics Conf. Ser., No. 171 (IOP publishing, Bristol, 2003) pp. R2.7.1–R2.7.7.
[79] C. Carlone, A. Beliveau, and N. L. Rowell, J. Lumin. **47**, 309 (1991).
[80] P. P. Paskov, P. O. Holtz, B. Monemar, J. M. Garcia, W. V. Schoenfeld, and P. M. Petroff, Appl. Phys. Lett. **77**, 812 (2000).
[81] V. Yu. Ivanov, Yu. G. Semenov, M. Surma, and M. Godlewski, Phys. Rev. B **54**, 4696 (1996).
[82] T. Itoh, M. Nishijima, A. I. Ekimov, C. Gourdon, Al. L. Efros, and M. Rosen, Phys. Rev. Lett. **74**, 1645 (1995).
[83] K. Kral, P. Zdenek, and Z. Khas, Surf. Sci. **566**, 321 (2004).
[84] J. R. Santos, M. I. Vasilevskiy, and S. A. Filonovich, Phys. Rev. B **78**, 245422 (2008).
[85] C. Zander and K. H. Drexhage, Cooling of Dye Solution by anti-Stokes Fluorescence, in: Advances in Photochemistry, edited by D. C. Neckers, D. H. Volman, and G. von Bunau (Wiley, New York, 1995), pp. 59–78.
[86] O. Kulakovich, N. Strekal, A. Yaroshevich, S. Maskevich, S. Gaponenko, I. Nabiev, U. Woggon, and M. Artemyev, Nano Lett. **2**, 1449 (2000).
[87] K. Ray, R. Badugu, and J. R. Lakowicz, J. Am. Chem. Soc. **128**, 8998 (2006).
[88] J. B. Khurgin, Phys. Rev. Lett. **98**, 177401 (2007).
[89] S. A. Ivanov, J. Nanda, P. Piryatinski, M. Achermann, L. P. Balet, I. V. Bezel, P. O. Anikeeva, S. Tretiak, and V. I. Klimov, J. Phys. Chem. B **108**, 10625 (2004).
[90] V. I. Klimov, S. A. Ivanov, J. Nanda, M. Achermann, I. Bezel, J. A. McGuire, and A. Piryatinski, Nature **447**, 441 (2007).